









## Multi-band Tractor Forced Photometry and Redshifts in the CDFS and XMM-LSS Fields

Kristina Nyland <sup>1</sup>, Mark Lacy <sup>2</sup>, W.N. Brandt <sup>3,4,5</sup>, Guang Yang <sup>6,7</sup>, Qingling Ni <sup>8</sup>, Anna Sajina <sup>9</sup>,  
Fan Zou <sup>3,4</sup> and Mattia Vaccari <sup>10</sup>

<sup>1</sup>*U.S. Naval Research Laboratory, 4555 Overlook Ave SW, Washington, DC 20375, USA*

<sup>2</sup>*National Radio Astronomy Observatory, Charlottesville, VA 22903, USA*

<sup>3</sup>*Department of Astronomy & Astrophysics, The Pennsylvania State University, University Park, PA 16802, USA*

<sup>4</sup>*Institute for Gravitation and the Cosmos, The Pennsylvania State University, University Park, PA 16802, USA*

<sup>5</sup>*Department of Physics, 104 Davey Lab, The Pennsylvania State University, University Park, PA 16802, USA*

<sup>6</sup>*Department of Physics and Astronomy, Texas A&M University, College Station, TX 77843-4242, USA*

<sup>7</sup>*George P. and Cynthia Woods Mitchell Institute for Fundamental Physics and Astronomy, Texas A&M University, College Station, TX 77843-4242, USA*

<sup>8</sup>*Institute for Astronomy, University of Edinburgh, Royal Observatory, Edinburgh, EH9 3HJ, UK*

<sup>9</sup>*Department of Physics and Astronomy, Tufts University, Medford, MA, 02155, USA*

<sup>10</sup>*Department of Astronomy, University of Cape Town, 7701 Rondebosch, Cape Town, South Africa*

### ABSTRACT

We present a catalog of multi-band forced photometry in the CDFS and XMM-LSS fields. We used *The Tractor* image-modeling software to produce de-blended photometry across 13 to 15 optical/infrared bands and determine photometric redshifts. Our catalog, which is publicly available on IRSA, contains  $\sim 1.5$  million sources and covers a total area of  $\sim 9$  deg<sup>2</sup>.

### BACKGROUND

Wide-field surveys are essential for characterizing basic galaxy properties such as redshift, stellar mass, and nuclear activity level. This requires accurate photometry across heterogeneous combinations of mixed-resolution surveys. Here, we present multi-band forced photometry using *The Tractor* (Lang et al. 2016) over 9 deg<sup>2</sup> in the CDFS and XMM-LSS fields. *The Tractor* employs position/shape priors from a high-resolution image and flexible PSF modeling to fit the source flux and shape properties in lower-resolution bands. Compared to position-matched catalogs, *The Tractor* produces de-blended *Spitzer*/IRAC fluxes that lead to more accurate photometric redshifts (Nyland et al. 2017).

### DATA PRODUCTS

Our photometry includes the 3.6 and 4.5  $\mu\text{m}$  *Spitzer*/DeepDrill (Lacy et al. 2021) bands; ground-based near-infrared data in the *Z*, *Y*, *J*, *H*, and *Ks* bands from VIDEO (Jarvis et al. 2013); and optical data in the *g*, *r*, *i*, and *z* bands from HSC (Miyazaki et al. 2012). In CDFS, deep archival HSC data are used (Ni et al. 2019), and in XMM-LSS, data from the HSC-SSP (Aihara et al. 2018) are used. In CDFS, the *u*, *g*, *r*, and *i* bands from VOICE (Vaccari et al. 2016) are included. In XMM-LSS, we also include *u'*-band data from CFHTLS (Gwyn 2012). The main differences between this study and Nyland et al. (2017) are (1) an increased image cutout size (20'') for improved extended source photometry and (2) iterative sigma clipping for image background statistics. For XMM-LSS, we limited the catalog to  $Ks < 23$ , as described in Krefting et al. (2020).

Photometric redshifts have been estimated for all sources, regardless of the SNR, and are taken directly from Chen et al. (2018) and Zou et al. (2021). The catalog is described in Table 1 and is publicly available on IRSA (Nyland, et al. 2023). Our catalog expands upon published studies using *The Tractor* by our team for the XMM-LSS field (Krefting et al. 2020), sources in CDFS and XMM-LSS detected in X-ray surveys (Chen et al. 2018; Zou et al. 2021; Ni et al. 2021; Zou et al. 2022), and faint sub-millimeter galaxies in XMM-LSS (Patil et al. 2019).

Table 1. Catalog description

Name	Description	Name	Description
ra	J2000 position	red_chi_Z_VIDEO	VIDEO $Z$ -band $\chi_{\text{red}}^2$
dec	J2000 position	red_chi_Y_VIDEO	VIDEO $Y$ -band $\chi_{\text{red}}^2$
field	XMM-LSS or CDFS	red_chi_I_HSC	HSC $i$ -band $\chi_{\text{red}}^2$
F_Ks_VIDEO	VIDEO $Ks$ -band flux	red_chi_R_HSC	HSC $r$ -band $\chi_{\text{red}}^2$
F_H_VIDEO	VIDEO $H$ -band flux	red_chi_G_HSC	HSC $g$ -band $\chi_{\text{red}}^2$
F_J_VIDEO	VIDEO $J$ -band flux	red_chi_Z_HSC	HSC $z$ -band $\chi_{\text{red}}^2$
F_Y_VIDEO	VIDEO $Y$ -band flux	red_chi_Y_HSC	HSC $Y$ -band $\chi_{\text{red}}^2$
F_Z_VIDEO	VIDEO $Z$ -band flux	red_chi_I_VOICE	VOICE $i$ -band $\chi_{\text{red}}^2$
F_I_HSC	HSC $i$ -band flux	red_chi_R_VOICE	VOICE $r$ -band $\chi_{\text{red}}^2$
F_R_HSC	HSC $r$ -band flux	red_chi_G_VOICE	VOICE $g$ -band $\chi_{\text{red}}^2$
F_G_HSC	HSC $g$ -band flux	red_chi_U_VOICE	VOICE $u$ -band $\chi_{\text{red}}^2$
F_Z_HSC	HSC $z$ -band flux	red_chi_U_CFHT	CFHTLS $u'$ -band $\chi_{\text{red}}^2$
F_Y_HSC	HSC $Y$ -band flux	red_chi_CH1	DeepDrill [3.6] $\chi_{\text{red}}^2$
F_I_VOICE	VOICE $i$ -band flux	red_chi_CH2	DeepDrill [4.5] $\chi_{\text{red}}^2$
F_R_VOICE	VOICE $r$ -band flux	skylevel_Ks_VIDEO	VIDEO $Ks$ -band skylevel
F_G_VOICE	VOICE $g$ -band flux	skylevel_H_VIDEO	VIDEO $H$ -band skylevel
F_U_VOICE	VOICE $u$ -band flux	skylevel_J_VIDEO	VIDEO $J$ -band skylevel
F_U_CFHT	CFHTLS $u'$ -band flux	skylevel_Z_VIDEO	VIDEO $Z$ -band skylevel
F_CH1	DeepDrill [3.6] flux	skylevel_Y_VIDEO	VIDEO $Y$ -band skylevel
F_CH2	DeepDrill [4.5] flux	skylevel_I_HSC	HSC $i$ -band skylevel
F_err_Ks_VIDEO	VIDEO $Ks$ -band flux error	skylevel_R_HSC	HSC $r$ -band skylevel
F_err_H_VIDEO	VIDEO $H$ -band flux error	skylevel_G_HSC	HSC $g$ -band skylevel
F_err_J_VIDEO	VIDEO $J$ -band flux error	skylevel_Z_HSC	HSC $z$ -band skylevel
F_err_Y_VIDEO	VIDEO $Y$ -band flux error	skylevel_Y_HSC	HSC $Y$ -band skylevel
F_err_Z_VIDEO	VIDEO $Z$ -band flux error	skylevel_I_VOICE	VOICE $i$ -band skylevel
F_err_I_HSC	HSC $i$ -band flux error	skylevel_R_VOICE	VOICE $r$ -band skylevel
F_err_R_HSC	HSC $r$ -band flux error	skylevel_G_VOICE	VOICE $g$ -band skylevel
F_err_G_HSC	HSC $g$ -band flux error	skylevel_U_VOICE	VOICE $u$ -band skylevel
F_err_Z_HSC	HSC $z$ -band flux error	skylevel_U_CFHT	CFHTLS $u'$ -band skylevel
F_err_Y_HSC	HSC $Y$ -band flux error	skylevel_CH1	DeepDrill [3.6] skylevel
F_err_I_VOICE	VOICE $i$ -band flux error	skylevel_CH2	DeepDrill [4.5] skylevel
F_err_R_VOICE	VOICE $r$ -band flux error	skynoise_Ks_VIDEO	VIDEO $Ks$ -band skynoise
F_err_G_VOICE	VOICE $g$ -band flux error	skynoise_H_VIDEO	VIDEO $H$ -band skynoise
F_err_U_VOICE	VOICE $u$ -band flux error	skynoise_J_VIDEO	VIDEO $J$ -band skynoise
F_err_U_CFHT	CFHTLS $u'$ -band flux error	skynoise_Z_VIDEO	VIDEO $Z$ -band skynoise
F_err_CH1	DeepDrill [3.6] flux error	skynoise_Y_VIDEO	VIDEO $Y$ -band skynoise
F_err_CH2	DeepDrill [4.5] flux error	skynoise_I_HSC	HSC $i$ -band skynoise
Mag_Ks_VIDEO	VIDEO $Ks$ -band magnitude	skynoise_R_HSC	HSC $r$ -band skynoise
Mag_H_VIDEO	VIDEO $H$ -band magnitude	skynoise_G_HSC	HSC $g$ -band skynoise
Mag_J_VIDEO	VIDEO $J$ -band magnitude	skynoise_Z_HSC	HSC $z$ -band skynoise
Mag_Y_VIDEO	VIDEO $Y$ -band magnitude	skynoise_Y_HSC	HSC $Y$ -band skynoise
Mag_Z_VIDEO	VIDEO $Z$ -band magnitude	skynoise_I_VOICE	VOICE $i$ -band skynoise
Mag_I_HSC	HSC $i$ -band magnitude	skynoise_R_VOICE	VOICE $r$ -band skynoise
Mag_R_HSC	HSC $r$ -band magnitude	skynoise_G_VOICE	VOICE $g$ -band skynoise
Mag_G_HSC	HSC $g$ -band magnitude	skynoise_U_VOICE	VOICE $u$ -band skynoise
Mag_Z_HSC	HSC $z$ -band magnitude	skynoise_U_CFHT	CFHTLS $u'$ -band skynoise
Mag_Y_HSC	HSC $Y$ -band magnitude	skynoise_CH1	DeepDrill [3.6] skynoise
Mag_I_VOICE	VOICE $i$ -band magnitude	skynoise_CH2	DeepDrill [4.5] skynoise
Mag_R_VOICE	VOICE $r$ -band magnitude	snr_Ks_VIDEO	VIDEO $Ks$ -band SNR
Mag_G_VOICE	VOICE $g$ -band magnitude	snr_H_VIDEO	VIDEO $H$ -band SNR
Mag_U_VOICE	VOICE $u$ -band magnitude	snr_J_VIDEO	VIDEO $J$ -band SNR
Mag_U_CFHT	CFHTLS $u'$ -band magnitude	snr_Z_VIDEO	VIDEO $Z$ -band SNR
Mag_CH1	DeepDrill [3.6] magnitude	snr_Y_VIDEO	VIDEO $Y$ -band SNR
Mag_CH2	DeepDrill [4.5] magnitude	snr_I_HSC	HSC $i$ -band SNR

Table 1 continued on next page

Table 1 (continued)

Name	Description	Name	Description
Mag_err_Ks_VIDEO	VIDEO <i>Ks</i> -band magnitude error	snr_R_HSC	HSC <i>r</i> -band SNR
Mag_err_H_VIDEO	VIDEO <i>H</i> -band magnitude error	snr_G_HSC	HSC <i>g</i> -band SNR
Mag_err_J_VIDEO	VIDEO <i>J</i> -band magnitude error	snr_Z_HSC	HSC <i>z</i> -band SNR
Mag_err_Y_VIDEO	VIDEO <i>Y</i> -band magnitude error	snr_Y_HSC	HSC <i>Y</i> -band SNR
Mag_err_Z_VIDEO	VIDEO <i>Z</i> -band magnitude error	snr_L_VOICE	VOICE <i>i</i> -band SNR
Mag_err_I_HSC	HSC <i>i</i> -band magnitude error	snr_R_VOICE	VOICE <i>r</i> -band SNR
Mag_err_R_HSC	HSC <i>r</i> -band magnitude error	snr_G_VOICE	VOICE <i>g</i> -band SNR
Mag_err_G_HSC	HSC <i>g</i> -band magnitude error	snr_U_VOICE	VOICE <i>u</i> -band SNR
Mag_err_Z_HSC	HSC <i>z</i> -band magnitude error	snr_U_CFHT	CFHTLS <i>u'</i> -band SNR
Mag_err_Y_HSC	HSC <i>Y</i> -band magnitude error	snr_CH1	DeepDrill [3.6] SNR
Mag_err_I_VOICE	VOICE <i>i</i> -band magnitude error	snr_CH2	DeepDrill [4.5] SNR
Mag_err_R_VOICE	VOICE <i>r</i> -band magnitude error	Model	Surface brightness profile model
Mag_err_G_VOICE	VOICE <i>g</i> -band magnitude error	Fiducial_Band	VIDEO band used to define Model
Mag_err_U_VOICE	VOICE <i>u</i> -band magnitude error	CFHTLS_tier	CFHTLS Tier (W1 or D1)
Mag_err_U_CFHT	CFHTLS <i>u'</i> -band magnitude error	HSC_tier	HSC-SSP Tier (Wide, Deep, or Ultradeep )
Mag_err_CH1	DeepDrill [3.6] magnitude error	Flag_I_HSC	HSC quality flag (1 == poor)
Mag_err_CH2	DeepDrill [4.5] magnitude error	Flag_R_HSC	HSC quality flag (1 == poor)
red_chi_Ks_VIDEO	VIDEO <i>Ks</i> -band $\chi^2_{\text{red}}$	Flag_G_HSC	HSC quality flag (1 == poor)
red_chi_H_VIDEO	VIDEO <i>H</i> -band $\chi^2_{\text{red}}$	Flag_Z_HSC	HSC quality flag (1 == poor)
red_chi_J_VIDEO	VIDEO <i>J</i> -band $\chi^2_{\text{red}}$	photo_z	Photometric redshift

NOTE—We report fluxes in  $\mu\text{Jy}$  and magnitudes AB. For information on errors, see Appendix A of Nyland et al. (2017). Model values may be Dev (deVaucouleurs), Exp (exponential), or PtSrc (point source).

## ACKNOWLEDGMENTS

Basic research in radio astronomy at the U.S. Naval Research Laboratory is supported by 6.1 Base Funding. The National Radio Astronomy Observatory is a facility of the National Science Foundation operated under cooperative agreement by Associated Universities, Inc.

## REFERENCES

- Aihara, H., Arimoto, N., Armstrong, R., et al. 2018, PASJ, 70, S4, doi: [10.1093/pasj/psx066](https://doi.org/10.1093/pasj/psx066)
- Chen, C.-T. J., Brandt, W. N., Luo, B., et al. 2018, MNRAS, 478, 2132, doi: [10.1093/mnras/sty1036](https://doi.org/10.1093/mnras/sty1036)
- Gwyn, S. D. J. 2012, AJ, 143, 38, doi: [10.1088/0004-6256/143/2/38](https://doi.org/10.1088/0004-6256/143/2/38)
- Jarvis, M. J., Bonfield, D. G., Bruce, V. A., et al. 2013, MNRAS, 428, 1281, doi: [10.1093/mnras/sts118](https://doi.org/10.1093/mnras/sts118)
- Krefting, N., Sajina, A., Lacy, M., et al. 2020, ApJ, 889, 185, doi: [10.3847/1538-4357/ab60a0](https://doi.org/10.3847/1538-4357/ab60a0)
- Lacy, M., Surace, J. A., Farrah, D., et al. 2021, MNRAS, 501, 892, doi: [10.1093/mnras/staa3714](https://doi.org/10.1093/mnras/staa3714)
- Lang, D., Hogg, D. W., & Schlegel, D. J. 2016, AJ, 151, 36, doi: [10.3847/0004-6256/151/2/36](https://doi.org/10.3847/0004-6256/151/2/36)
- Miyazaki, S., Komiyama, Y., Nakaya, H., et al. 2012, in Society of Photo-Optical Instrumentation Engineers (SPIE) Conference Series, Vol. 8446, Ground-based and Airborne Instrumentation for Astronomy IV, ed. I. S. McLean, S. K. Ramsay, & H. Takami, 84460Z, doi: [10.1117/12.926844](https://doi.org/10.1117/12.926844)
- Ni, Q., Timlin, J., Brandt, W. N., & Yang, G. 2019, Research Notes of the American Astronomical Society, 3, 5, doi: [10.3847/2515-5172/aaf8af](https://doi.org/10.3847/2515-5172/aaf8af)
- Ni, Q., Brandt, W. N., Chen, C.-T., et al. 2021, ApJS, 256, 21, doi: [10.3847/1538-4365/ac0dc6](https://doi.org/10.3847/1538-4365/ac0dc6)
- Nyland, K., Lacy, M., Sajina, A., et al. 2017, ApJS, 230, 9, doi: [10.3847/1538-4365/aa6fed](https://doi.org/10.3847/1538-4365/aa6fed)
- Nyland, et al. 2023, DeepDrill Forced Photometry Catalog, IPAC, doi: [10.26131/IRSA550](https://doi.org/10.26131/IRSA550)
- Patil, P., Nyland, K., Lacy, M., et al. 2019, ApJ, 871, 109, doi: [10.3847/1538-4357/aaf7a4](https://doi.org/10.3847/1538-4357/aaf7a4)

Vaccari, M., Covone, G., Radovich, M., et al. 2016, in The 4th Annual Conference on High Energy Astrophysics in Southern Africa (HEASA 2016), 26, doi: [10.22323/1.275.0026](https://doi.org/10.22323/1.275.0026)

Zou, F., Yang, G., Brandt, W. N., et al. 2021, Research Notes of the American Astronomical Society, 5, 56, doi: [10.3847/2515-5172/abf050](https://doi.org/10.3847/2515-5172/abf050)

Zou, F., Brandt, W. N., Chen, C.-T., et al. 2022, ApJS, 262, 15, doi: [10.3847/1538-4365/ac7bdf](https://doi.org/10.3847/1538-4365/ac7bdf)